



# In-situ structural studies of manganese spinel-based cathode materials



Łukasz Kondracki, Andrzej Kulka, Anna Milewska, Janina Molenda\*

AGH University of Science and Technology, Faculty of Energy and Fuels, Department of Hydrogen Energy, al. A. Mickiewicza 30, 30-059 Krakow, Poland

## ARTICLE INFO

### Article history:

Received 7 November 2016  
Received in revised form 16 December 2016  
Accepted 4 January 2017  
Available online 4 January 2017

### Keywords:

Li-ion batteries  
cathode materials  
Ni, Cu- substituted manganese spinel  
In-situ XRD

## ABSTRACT

In this paper a detailed *in-situ* XRD investigation of structural properties as well as lithium diffusion coefficient determination of  $\text{LiMn}_2\text{O}_4$ ,  $\text{LiMn}_{1.5}\text{Ni}_{0.5}\text{O}_4$  and  $\text{LiMn}_{1.5}\text{Ni}_{0.45}\text{Cu}_{0.05}\text{O}_4$  cathode materials are presented. Kinetics of  $\text{Li}^+$  intercalation/deintercalation mechanism are corroborated with structural changes of the cathode materials during electrochemical reactions. It was found that substitution of Mn by Ni and Cu in  $\text{LiMn}_2\text{O}_4$  ions leads to single-phased electrochemical operational mechanism in  $\text{Li}_x\text{Mn}_{1.5}\text{Ni}_{0.45}\text{Cu}_{0.05}\text{O}_4$  in the whole examined lithium concentration range.

© 2017 Elsevier Ltd. All rights reserved.

## 1. Introduction

The great interest in  $\text{LiMn}_2\text{O}_4$  manganese spinel results from the market's demand for an efficient technology of cathodes for Li-ion batteries [1–3]. Its reversible capacity is comparable to  $\text{LiCoO}_2$  (up to 130 mAh/g), but manganese spinel is cheaper and more environmentally friendly. The drawback of the undoped  $\text{LiMn}_2\text{O}_4$  as a cathode material is significant capacity fading of a Li-ion cell containing  $\text{LiMn}_2\text{O}_4$ -based electrode. This is believed to be a synergy of several effects: thermal decomposition of  $\text{LiPF}_6$ -based carbonate electrolytes, manganese dissolution via the disproportionation reaction, crystal phase transition due to Jahn–Teller distortion, oxygen deficiency, loss of crystallinity and development of micro-strain during cycling [4,5]. One of the ways to suppress the Jahn–Teller distortion of lithium manganese spinel is substitution of Mn ions with other ions with different valence state –  $\text{Li}_x\text{M}_y\text{Mn}_{2-y}\text{O}_4$  ( $M = \text{Al, Mg, Ti, V, Cr, Fe, Co, Ni, Cu, Zn}$ ) [6–14]. These substitutions stabilize the structure of spinel, but at the same time reduce the 4 V – capacity related to redox reaction  $\text{Mn}^{3+}/\text{Mn}^{4+}$ . On the other hand, by appropriate substitution strategy one can obtain materials exhibiting redox reactions around 5 V vs.  $\text{Li}^+/\text{Li}^0$ .

The intercalation of lithium ions into the crystal structure of the host is strictly connected with introduction of the same number of electrons into the electronic structure of electrode material (ambipolar diffusion). Thus, the electronic structure of the electrodes is very important factor, which influences potential of

the electrode's reaction (voltage of the cell), as well as structural distortions or transitions [12,15–17]. Several studies have employed X-ray absorption and emission spectroscopy, a methods that give a direct access to electronic structure, to better understand the correlation between spinel-based electrode performance and its composition [18,19].

The lithium intercalation/deintercalation process from undoped  $\text{LiMn}_2\text{O}_4$  is well-described in the literature, but most of the works focuses solely on the electrochemical investigation of the electrode reactions, while omitting the structural changes of the material during cycling. Depending on the literature reference, the process of lithium deintercalation from undoped lithium manganese spinel  $\text{Li}_x\text{Mn}_2\text{O}_4$  is described in several different ways [20–22]. However, it is generally accepted that lithium deintercalation is single-phased up to certain  $x_{\text{Li}}$ , after which the mechanism changes to two-phased with Li-rich and Li-poor phases. It should be noted, that during the entire course of the process, the  $\text{Mn}_2\text{O}_4$ -core structure does not change in a significant way. Recent reports of precise operando neutron diffraction studies [23] indicate, that for the composition close to  $\text{Li}_{0.5}\text{Mn}_2\text{O}_4$  a reduction of symmetry is shown and indexed as  $P2_13$  space group.

Partial substitution of manganese by 0.5 mole of nickel ions lead to promising cathode for high energy Li-ion batteries- $\text{LiMn}_{1.5}\text{Ni}_{0.5}\text{O}_4$  exhibiting voltage potential equal 4.7 V vs.  $\text{Li}/\text{Li}^+$  and stability of crystal structure during the electrochemical reactions [24].  $\text{LiMn}_{1.5}\text{Ni}_{0.5}\text{O}_4$  similarly to undoped  $\text{LiMn}_2\text{O}_4$  manganese spinel is believed to undergo single-phased lithium intercalation/deintercalation reactions up to certain lithium content after which mechanism changes to two-phased one [25].

\* Corresponding author.

E-mail address: [molenda@agh.edu.pl](mailto:molenda@agh.edu.pl) (J. Molenda).

Several attempts to substitute manganese by copper in  $\text{Li}_x\text{Mn}_{2-y}\text{Cu}_y\text{O}_4$  in order to employ a voltage potential 4.4 V vs.  $\text{Li}/\text{Li}^+$  corresponding to  $\text{Cu}^{2+}/\text{Cu}^{3+}$  redox couple were reported [17,26,27]. Larger substitution level ( $y$  about 0.5 mole) of Cu in  $\text{Li}_x\text{Mn}_{2-y}\text{Cu}_y\text{O}_4$  triggers single phase mechanism of lithium deintercalation in the whole available Li concentration range [26]. Thus the aim of this work was investigation of influence of substitution of Mn ions by Ni and/or Cu ions on deintercalation/intercalation mechanisms in  $\text{LiMn}_2\text{O}_4$ ,  $\text{LiMn}_{1.5}\text{Ni}_{0.5}\text{O}_4$  and  $\text{LiMn}_{1.5}\text{Ni}_{0.45}\text{Cu}_{0.05}\text{O}_4$  cathode materials.

## 2. Experimental

$\text{LiMn}_2\text{O}_4$ ,  $\text{LiMn}_{1.5}\text{Ni}_{0.5}\text{O}_4$  and  $\text{LiMn}_{1.5}\text{Ni}_{0.45}\text{Cu}_{0.05}\text{O}_4$  manganese spinels were synthesized using a sol-gel method [28]. Soluble acetates  $\text{Mn}(\text{CH}_3\text{COO})_2 \cdot 4\text{H}_2\text{O}$ ,  $\text{Ni}(\text{CH}_3\text{COO})_2 \cdot 4\text{H}_2\text{O}$  and nitrates  $\text{LiNO}_3$ ,  $\text{Cu}(\text{NO}_3)_2 \cdot 3\text{H}_2\text{O}$  were taken as precursors in proper stoichiometry. The substrates were dissolved in small amount of deionized water. A solution of ammonia was added to reach  $\text{pH}=9$ . The obtained sols were dried at  $90^\circ\text{C}$  for 48 h, then calcined at  $300^\circ\text{C}$  for 24 h and pelletized. The pellets were then annealed in air at  $800^\circ\text{C}$  for 6 h followed by quenching to room temperature.

Phase composition and crystal structure of the samples were investigated using the XRD technique. Measurements were performed on a Panalytical Empyrean diffractometer in the 10–110 degree range using  $\text{CuK}\alpha$  radiation. Data were refined by the Rietveld method with GSAS/EXPGUI set of software [29].

Composite cathode layers, suitable for *in-situ* XRD measurements, were coated on a thin Al foil. The composite cathodes were prepared as a mixture of spinel powder, carbon black, polyvinylidene fluoride (in the weight ratio of 85:7.5:7.5), with N-methyl pyrrolidone in a slurry. *In-situ* XRD measurements were conducted in the 20–70 degree on Panalytical Empyrean diffractometer. A custom-made gas-tight cell for these studies was made from Teflon and stainless steel containers, joint by screws and sealed by gaskets. A Beryllium window, was used as an X-ray transparent medium and a current collector at the same time [30].

Calibration of the position of the layer in relation to the diffractometer's geometry, was done by comparing initial *in-situ* patterns to the ex-situ XRD data of identical  $\text{Li}_x\text{Mn}_{1.5}\text{Ni}_{0.5-y}\text{Cu}_y\text{O}_4$ -based layers. The electrochemical tests during *in-situ* XRD measurements were performed using an Autolab PGSTAT302N potentiostat/galvanostat. The charge/discharge rate was set to C/10. Rate of a single measurement of an XRD pattern was set to be 30 min long. Such obtained patterns were then analyzed using the mentioned GSAS/EXPGUI set of software. To evaluate the quality of fit, the analysis of Rietveld discrepancy values, i.e. ranges of  $\chi^2$ , and weighted profile R-factors [31] for fitted curve and background ( $R_{\text{wp}}^{\text{f}}$  and  $R_{\text{wp}}^{\text{b}}$  respectively) for each composition are shown in Table 1. Lithium diffusion coefficient was determined by GITT technique [32] in CR-2032  $\text{Li}/\text{Li}^+/\text{Li}_x\text{Mn}_2\text{O}_4$ ,  $\text{Li}/\text{Li}^+/\text{Li}_x\text{Mn}_{1.5}\text{Ni}_{0.5}\text{O}_4$  and  $\text{Li}/\text{Li}^+/\text{Li}_x\text{Mn}_{1.5}\text{Ni}_{0.45}\text{Cu}_{0.05}\text{O}_4$  cells.

**Table 1**

The analysis of Rietveld discrepancy values: ranges of  $\chi^2$ , and R factors obtained during *in-situ* measurements of  $\text{Li}/\text{Li}^+/\text{Li}_x\text{Mn}_{1.5}\text{Ni}_{0.5-y}\text{Cu}_y\text{O}_4$  cells.

Examined cathode material	$\chi^2$	weighted profile R-factors	
		fitted $R_{\text{wp}}^{\text{f}}$	background $R_{\text{wp}}^{\text{b}}$
$\text{Li}_x\text{Mn}_2\text{O}_4$	1.656– 2.394	0.0157– 0.0189	0.0249–0.0331
$\text{Li}_x\text{Mn}_{1.5}\text{Ni}_{0.5}\text{O}_4$	2.104– 3.389	0.0166– 0.0211	0.0183–0.0342
$\text{Li}_x\text{Mn}_{1.5}\text{Ni}_{0.45}\text{Cu}_{0.05}\text{O}_4$	1.735–2.416	0.0150– 0.0177	0.0237–0.0246

## 3. Results and Discussion

### 3.1. Pristine materials characterization

Firstly, the structural properties of the as-synthesized three samples;  $\text{LiMn}_2\text{O}_4$ ,  $\text{LiMn}_{1.5}\text{Ni}_{0.5}\text{O}_4$  and  $\text{LiMn}_{1.5}\text{Ni}_{0.45}\text{Cu}_{0.05}\text{O}_4$  were characterized. The analysis of the intensity and full width at half maximum (FWHM) of X-ray reflection peaks confirmed that the all materials were well crystallized. In case of each sample all the reflection peaks of the main phase could be indexed with cubic Fd-3m group. Detailed analysis revealed that, the  $\text{LiMn}_2\text{O}_4$  was single phased, while Ni-containing materials exhibit some very small amounts of impurities that can be indexed as  $\text{Ni}_x\text{O}$  rock salt phase. The XRD patterns are shown in Fig. 1 with the impurities marked with an (\*) symbol. As reported,  $\text{LiMn}_{1.5}\text{Ni}_{0.5}\text{O}_4$  can crystallize in two distinct P4<sub>3</sub>32 and Fd-3m space groups [33,34] due to the 3d metal arrangement.

Cations distribution for this material depends on the synthesis conditions: materials annealed at lower temperature (below  $700^\circ\text{C}$ ) adopt a primitive cubic structure (P4<sub>3</sub>32) with ordering in the 3d metal sublattice [35]. Samples treated at temperature higher than  $700^\circ\text{C}$  are generally reported to crystallize in the Fd-3m [24,25]. Since all the examined materials were annealed at  $800^\circ\text{C}$ , pristine  $\text{LiMn}_{1.5}\text{Ni}_{0.5}\text{O}_4$  exhibits higher symmetry of Fd-3m group. Additionally, it was found that introduction of Cu ions into spinel structure increases the cations position mixing between Li and 3d metals as can be observed by comparing the intensity ratios of the (400)/(311) peaks of  $\text{LiMn}_{1.5}\text{Ni}_{0.5}\text{O}_4$  and  $\text{LiMn}_{1.5}\text{Ni}_{0.45}\text{Cu}_{0.05}\text{O}_4$ . The ratios represent the cation mixing between octahedral and tetrahedral sites in the spinel structure – the lower the parameter, the stronger the effect is [17] (for ratio around 1, the mixing does not occur). Refined lattice cell parameters of the examined materials are shown in Table 2 and are in good agreement with the literature.

### 3.2. Lithium intercalation/deintercalation mechanism in $\text{Li}_x\text{Mn}_2\text{O}_4$ and $\text{Li}_x\text{Mn}_{1.5}\text{Ni}_{0.5}\text{O}_4$

*In-situ* XRD data for investigated  $\text{Li}/\text{Li}^+/\text{Li}_x\text{Mn}_2\text{O}_4$  and  $\text{Li}/\text{Li}^+/\text{Li}_x\text{Mn}_{1.5}\text{Ni}_{0.5}\text{O}_4$  cells were recorded in subsequent single scans during constant charge of the cells with C/10 current rate. The enlarged range of 35–40° of the XRD patterns with corresponding discharge curves for Li-ion batteries containing  $\text{Li}_x\text{Mn}_2\text{O}_4$  and  $\text{Li}_x\text{Mn}_{1.5}\text{Ni}_{0.5}\text{O}_4$  electrodes are shown in Figs. 2 and 3 respectively.

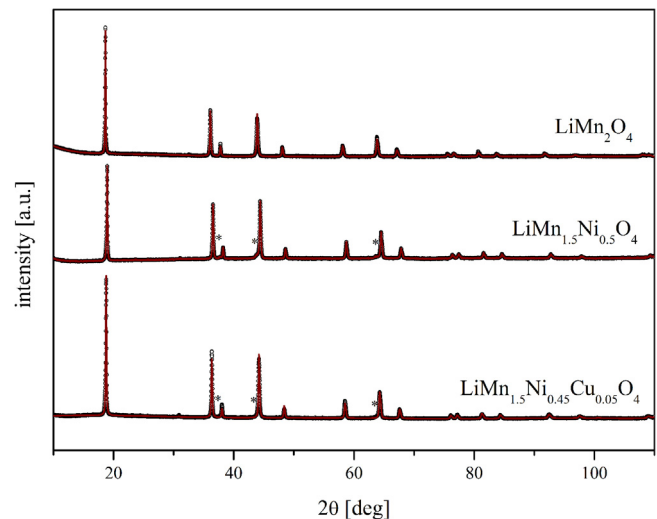


**Fig. 1.** XRD patterns of pristine materials.

Download English Version:

<https://daneshyari.com/en/article/6472228>

Download Persian Version:

<https://daneshyari.com/article/6472228>

[Daneshyari.com](https://daneshyari.com)